Trans. Japan Soc. Aero. Space Sci.
Vol. 64, No. 3, pp. 125–135, 2021
DOI: 10.2322/tjsass.64.125

Sounding the Atmospheric Density at the Altitude of LARES and Ajisai during Solar Cycle 24*

Carmen PARDINI,[1)†] Luciano ANSELMO,[1)] David M. LUCCHESI,[1),2),3)] Roberto PERON,[2),3)] Massimo BASSAN,[3),4)] Carmelo MAGNAFICO,[2),3)] Giuseppe PUCACCO,[3),4)] and Massimo VISCO[2),3)]

[1)]*Institute of Information Science and Technologies (ISTI), National Research Council (CNR), Pisa 56124, Italy*
[2)]*Institute for Space Astrophysics and Planetology (IAPS), National Institute of Astrophysics (INAF), Rome 00133, Italy*
[3)]*National Institute of Nuclear Physics (INFN), Section of Rome Tor Vergata, Rome 00133, Italy*
[4)]*Physics Department, University of Rome Tor Vergata, Rome 00133, Italy*

During Solar Cycle 24, the passive spherical satellites LARES and Ajisai, placed in nearly circular orbits with mean geodetic altitudes between 1450 and 1500 km, were used as powerful tools to probe the neutral atmosphere density and the performances of six thermospheric models in orbital regimes for which the role of dominant atomic species is contended by hydrogen and helium, and accurate satellite measurements are scarce. The starting point of the analysis was the accurate determination of the secular semi-major axis decay rate and the corresponding neutral drag acceleration in a satellite-centered orbital system. Then, for each satellite, thermospheric model and solar activity level, the drag coefficients capable of reproducing the orbital decay observed were found. These coefficients were finally compared with the physical drag coefficients computed for both satellites in order to assess the biases affecting the thermospheric density models. None of them could be considered unconditionally the best; the specific outcome depending on solar activity and the regions of the atmosphere crossed by the satellites. During solar maximum conditions, an additional density bias linked to the satellite orbit inclination was detected.

Key Words: Neutral Drag, Thermospheric Density Models, Solar Cycle 24, LARES, Ajisai

Nomenclature

a: semi-major axis, m
A: satellite average cross-section, m^2
C_D: drag coefficient
C_{DF}: physical drag coefficient
$C_{D\mathrm{H}}$: drag coefficient for the H species
$C_{D\mathrm{He}}$: drag coefficient for the He species
$C_{D\mathrm{O}}$: drag coefficient for the O species
$F_{10.7}$: solar radio flux at 10.7 cm, sfu
$\boldsymbol{F}_D$: drag force, N
h: satellite geodetic altitude, km
H: hydrogen atom
He: helium atom
i: orbital inclination, $^\circ$
M: molar mass, g/mol
M_S: satellite mass, kg
n: orbital mean motion, rad s^{-1}
n_{H}: H atmospheric number density, cm^{-3}
n_{He}: He atmospheric number density, cm^{-3}
n_{O}: O atmospheric number density, cm^{-3}
O: oxygen atom
R: gas constant, $= 8.314\,J\,mol^{-1}\,K^{-1}$
R_D: drag radial component, $m\,s^{-2}$
sfu: solar flux unit, $10^{-22}\,W\,m^{-2}\,Hz^{-1}$
Si: silicon atom
t: time, s
T: atmospheric temperature, K
T_D: drag transverse component, $m\,s^{-2}$
T_{exo}: exospheric temperature, K
V: satellite speed w.r.t. the atmosphere, $m\,s^{-1}$
V_m: most probable molecular speed, $m\,s^{-1}$
W: tungsten atom
W_D: drag normal component, $m\,s^{-2}$
α: δ accommodation coefficient
δ: C_D accommodation factor
φ: geocentric latitude, $^\circ$
μ: ratio of the atmospheric constituent atomic mass to that of the material which makes up the surface of the satellite
ρ: atmospheric density, $g\,cm^{-3}$
σ: standard deviation
$^\circ$: degree
$\langle\cdots\rangle$: mean of the parameter between brackets

1. Introduction

The primary objective of the Laser Relativity Satellite (LARES) mission is to improve the measurement accuracy of some general relativity effects, in particular that of Lense-Thirring,[1–4)] thereby providing significant contributions in the geodynamics and geodesy fields. In view of the main goal, this spherical satellite, with a radius of

*Presented at the 32nd International Symposium on Space Technology and Science & 9th Nano-Satellite Symposium, 15–21 June 2019, Fukui, Japan.
Received 25 June 2019; final revision received 22 July 2020; accepted for publication 10 September 2020.
†Corresponding author, carmen.pardini@isti.cnr.it

18.2 cm and a mass of 386.80 kg, made of tungsten alloy and uniformly hosting 92 fused silica (Suprasil®) corner cube laser retroreflectors on its surface, was designed in order to minimize the effects of non-gravitational perturbations, making LARES the densest artificial object ever launched into space.[5] Placed in a nearly circular orbit with an altitude of about 1454 km, inclined by 69.5°, and characterized by an extremely low area-to-mass-ratio (2.69×10^{-4} m^2/kg), the satellite was not expected to be substantially affected by non-conservative forces.

Nevertheless, thanks to precise orbit determinations based on the laser ranging data of LARES provided by the International Laser Ranging Service (ILRS),[6] it was possible to detect a very small secular semi-major axis decay, which was consistent with a non-conservative net force acting nearly opposite to the velocity vector of the satellite (i.e., a drag-like effect).[7,8]

As such drag-like effect might be ascribable to neutral atmosphere drag, the accurate knowledge of the observed accelerations may be assumed to be the starting point for probing, with LARES, the behavior of the neutral atmosphere under different environmental conditions, as well as exploring orbital regimes for which the dominant atomic species are helium and hydrogen, and accurate satellite measurements are scarce. The effect of the neutral drag perturbation in the first 3.7 years of the mission, from April 6, 2012 to December 25, 2015, had been investigated in a previous analysis,[7] indicating that nearly 99% of the secular semi-major axis decay observed was due to neutral atmosphere drag.

In support of such a relevant contribution of neutral drag at the altitude of LARES, the orbital decay of another passive spherical satellite, Ajisai, just 40 km higher than LARES but at an inclination of 50.0° and with an area-to-mass-ratio 19.70 times greater (5.30×10^{-3} m^2/kg), was investigated in the same interval of time as well.[8] With a diameter of 215 cm and a mass of 685.2 kg, this hollow sphere was much more sensitive to non-gravitational perturbations like atmospheric drag and radiative forces. It therefore represented an optimal target for comparative investigations of drag-like perturbations near the altitude of LARES. The surface of Ajisai is basically silica (SiO_2) in composition, being completely covered with 318 mirrors for reflecting sunlight and 1436 quartz corner cube retroreflectors for reflecting laser beams.[9]

This paper extends our previous analyses to the first 6.6 years of the LARES mission, from April 6, 2012 to October 26, 2018; in particular, highlighting the impact of the space weather conditions on the results obtained. The first interval, from April 6, 2012 to December 25, 2015, centered around the maximum of Solar Cycle 24. The second interval, from December 25, 2015 to October 26, 2018, corresponded to the declining phase and the deep minimum of the same cycle. The neutral drag perturbation, acting on both LARES and Ajisai, was investigated using an updated version of the SATRAP orbit propagator,[10,11] accounting for the real evolution of the space weather conditions. Among the many atmospheric density models implemented in SATRAP, the following six were applied in this study: Jacchia-Roberts 1971 (JR-71),[12] the Mass Spectrometer and Incoherent Scatter Radar Model 1986 (MSIS-86),[13] the Mass Spectrometer and Incoherent Scatter Radar Extended Model 1990 (MSISE-90),[14] NRLMSISE-00, developed at the US Naval Research Laboratory (NRL),[15,16] GOST2004, issued by the State Committee on Standardization and Metrology of the Russian Federation,[17] and Jacchia-Bowman 2008 (JB2008).[18]

2. Space Environment during Solar Cycle 24

Figure 1 shows the solar radio flux at 10.7 cm (2800 MHz) measured during the last two activity cycles (i.e., 23 and 24) of the Sun. The daily values and the averages over three solar rotations (81 days) are reported in solar flux units (sfu). This radio flux is the most widely used proxy for solar activity and all of the atmospheric models mentioned at the end of the previous section make use of it to properly represent the density variations of the thermosphere as a function of the varying emission of extreme ultraviolet radiation from the Sun. The dashed boxes identify the two time intervals for which the analyses described in this paper were carried out. An enlargement of the flux observed is presented in Fig. 2.

It should be noted that the LARES mission, started at the beginning of 2012, has so far taken place completely within Solar Cycle 24, which was also the weakest one recorded since the beginning of the 2800-MHz daily flux measurements at Penticton, British Columbia in 1947. Finally,

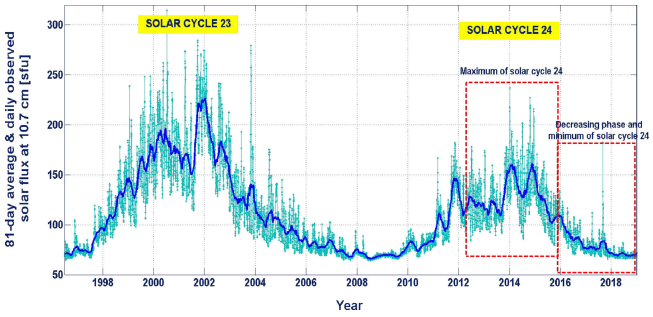

Fig. 1. Solar radio flux at 10.7 cm measured during the last two activity cycles of our star.
The daily measurements and their running averages over three solar rotations (81 days) are reported.

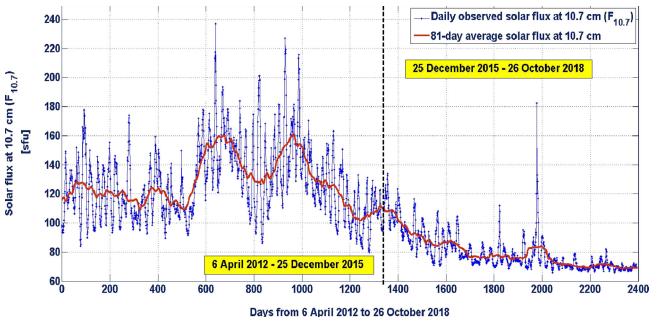

Fig. 2. Enlargement of the solar radio flux observed at 10.7 cm included in the two dashed boxes of Fig. 1.
The analyses presented in this paper relate to the two time intervals separated by the vertical dashed line.

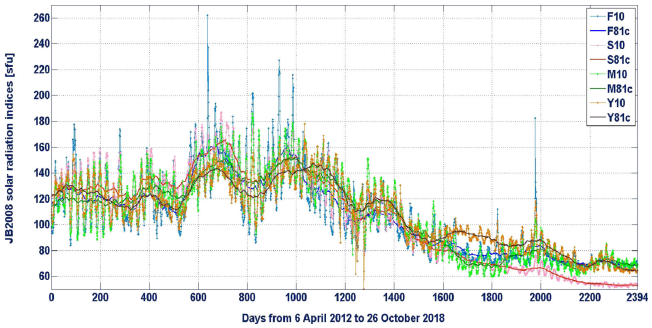

Fig. 3. Representation of the solar flux proxies used by the JB2008 thermospheric density model during the time span in which the study presented in this paper was carried out.

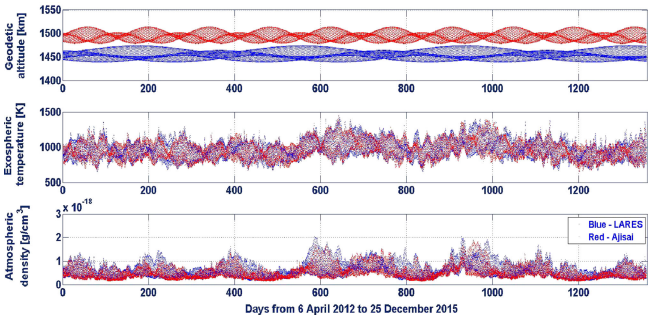

Fig. 4. Geodetic altitude of LARES and Ajisai, and corresponding exospheric temperature and atmospheric density from April 6, 2012 to December 25, 2015, centered around the maximum of Solar Cycle 24.

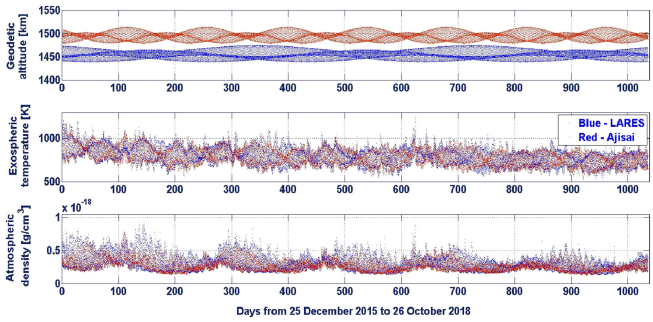

Fig. 5. Geodetic altitude of LARES and Ajisai, and corresponding exospheric temperature and atmospheric density from December 25, 2015 to October 26, 2018, during the declining phase and the minimum of Solar Cycle 24.

Fig. 3 shows, during the same time span analyzed and shown in Fig. 2, the full set of solar activity proxies used by the JB2008 atmospheric density model,[19,20] in addition to the daily and averaged values of $F_{10.7}$.

For the two time intervals in which neutral drag modeling was carried out centered around the maximum of Solar Cycle 24, April 6, 2012 to December 25, 2015 and December 25, 2015 to October 26, 2018, during the declining phase and the low minimum of the same cycle, Figs. 4 and 5 plot the geodetic altitude of LARES and Ajisai, and the corresponding exospheric temperature and atmospheric density for the two satellites. Figures 6 and 7 show the concentration of the three main atomic species: helium, hydrogen and oxygen.

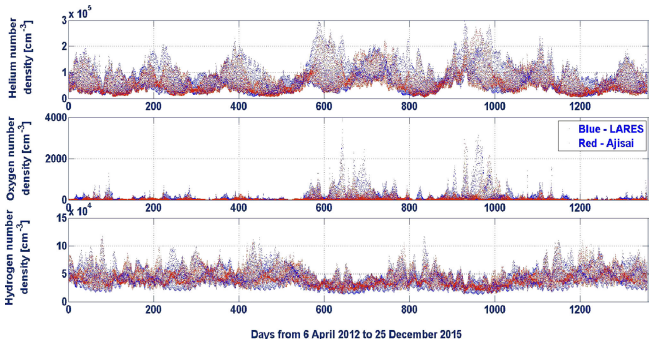

Fig. 6. Concentration of the three main atomic species (i.e., helium, hydrogen and oxygen) at the altitude of LARES and Ajisai from April 6, 2012 to December 25, 2015, centered around the maximum of Solar Cycle 24.

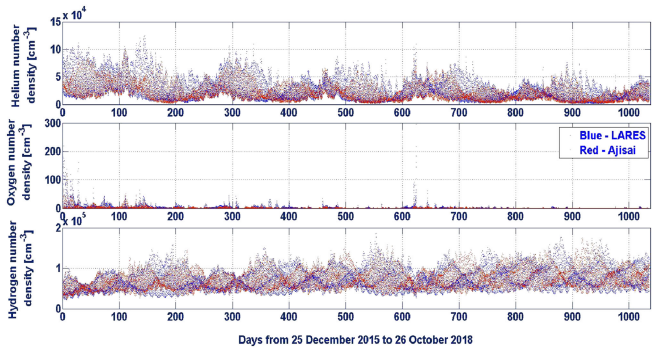

Fig. 7. Concentration of the three main atomic species (i.e., hydrogen, helium and oxygen) at the altitudes of LARES and Ajisai from December 25, 2015 to October 26, 2018, during the declining phase and the minimum of Solar Cycle 24.

Table 1. Average atmospheric properties along the orbits of LARES from April 6, 2012 to December 25, 2015.

Physical parameters	Mean values in the time span
Geodetic altitude	1454 km
Exospheric temperature	971 K
Atmospheric density	5.89×10^{-19} g/cm^3
H number density	4.17×10^4 cm^{-3}
He number density	7.36×10^4 cm^{-3}
O number density	9.16×10^1 cm^{-3}

All of these figures were obtained using the NRLMSISE-00 model. The average values found are listed in Tables 1 (LARES, around the solar cycle maximum), 2 (Ajisai, around the solar cycle maximum), 3 (LARES, during the solar cycle decrease and minimum), and 4 (Ajisai, during the solar cycle decrease and minimum).

In the time interval centered around the solar maximum, the dominant atmospheric atomic species at the altitudes of the two satellites was He (>60%), while when the exospheric temperature decreased, by about 175 K on average, during the declining and minimum phases of the solar cycle, the dominant atomic species was H (around 75%), and the overall mean atmospheric density diminished by 47%. The total period considered for the analysis was well representative of the varying environmental conditions encountered during a full solar activity cycle, even though very high activity lev-

Table 2. Average atmospheric properties along the orbits of Ajisai from April 6, 2012 to December 25, 2015.

Physical parameters	Mean values in the considered time span
Geodetic altitude	1494 km
Exospheric temperature	960 K
Atmospheric density	5.21×10^{-19} g/cm^3
H number density	4.25×10^{4} cm^{-3}
He number density	6.51×10^{4} cm^{-3}
O number density	5.46×10^{1} cm^{-3}

Table 3. Average atmospheric properties along the orbits of LARES from December 25, 2015 to October 26, 2018.

Physical parameters	Mean values in the time span
Geodetic altitude	1454 km
Exospheric temperature	796 K
Atmospheric density	3.11×10^{-19} g/cm^3
H number density	7.10×10^{4} cm^{-3}
He number density	2.64×10^{4} cm^{-3}
O number density	1.96×10^{0} cm^{-3}

Table 4. Average atmospheric properties along the orbits of Ajisai from December 25, 2015 to October 26, 2018.

Physical parameters	Mean values in the time span
Geodetic altitude	1494 km
Exospheric temperature	784 K
Atmospheric density	2.78×10^{-19} g/cm^3
H number density	7.17×10^{4} cm^{-3}
He number density	2.19×10^{4} cm^{-3}
O number density	9.77×10^{-1} cm^{-3}

els were not experienced for more than a few days, Cycle 24 being particularly weak.

3. Semi-Major Axis Decay

The semi-major axis decay analysis for the two satellites, presented elsewhere for the first 3.7 years,[7,8] was repeated and extended here over 6.6 years. The decay rate of LARES was obtained by processing the laser ranging information (i.e., normal points) provided by the ILRS with the NASA/GSFC software package GEODYN II.[21,22] The observables were fitted over 7-day orbit arcs and the precise orbit determination process uncovered the details of the semi-major axis secular decrease (Fig. 8). Since the launch, the mean semi-major axis of the satellite diminished by a little more than 5 m. During the period from April 6, 2012 to December 25, 2015 (i.e., 1358 days, 3.72 years), centered around the maximum of Solar Cycle 24, the average secular decay rate was 2.74 mm/d (i.e., 1.00 m per year), revealing the action of a non-conservative net force on the satellite, with a mean transverse acceleration component of -1.444×10^{-11} m/s^2. This was obtained by applying the classical relationship $T_D \cong (n/2) \times (\mathrm{d}a/\mathrm{d}t)$, where n is the satellite mean motion, a the semi-major axis and t the time.[23] During the period from December 25, 2015 to October 26, 2018 (1036 days, 2.84 years), which was the declining phase and low minimum of the same cycle, the average secular decay rate was 1.50 mm/d (i.e., 0.55 m per year), corresponding to a mean transverse acceleration component of -7.900×10^{-12} m/s^2.

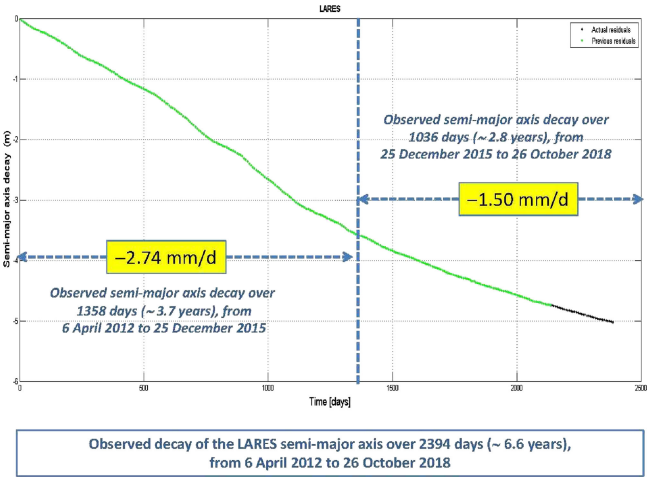

Fig. 8. Semi-major axis decay of LARES determined over 2394 days, from April 6, 2012 to October 26, 2018.
The laser ranging data was processed using GEODYN II.

The orbital decay of Ajisai due to the drag of neutral atmosphere has been known since its launch, and has been used over the years to check the predictions of several thermospheric density models under various conditions of solar and geomagnetic activity.[24–26] Concerning the present study, the average secular decrease of the semi-major axis of the satellite was obtained using SATRAP to analyze the two-line element sets determined by the US Strategic Command and issued by the Space Track Organization.[27,28] During the period from April 6, 2012 to December 25, 2015, centered around the maximum of Solar Cycle 24, the average secular decay rate was 38.44 mm/d (i.e., 14.04 m per year), corresponding to a mean transverse acceleration component of -2.013×10^{-10} m/s^2. From December 25, 2015 to October 26, 2018, during the declining phase and low minimum of the same cycle, the average secular decay rate was 24.48 mm/d (i.e., 8.94 m per year), corresponding to a mean transverse acceleration component of -1.282×10^{-10} m/s^2.

Therefore, even though Ajisai was 40 km higher than LARES, its greater area-to-mass ratio, by a factor of nearly 20, led to significantly larger mean along-track drag-like accelerations: by almost 14 times during the first period, and by more the 16 times during the second one. As a consequence, Ajisai was much more sensitive to thermospheric neutral drag than LARES, and also to other non-gravitational perturbations. However, the orbit determinations of the latter were so accurate, making both satellites powerful and complementary probes to investigate the properties of the atmosphere at those heights.

4. Neutral Atmosphere Drag Modeling

The most revealing feature of the drag force, which for a spherical body with uniform surface properties is directed opposite to the satellite's velocity relative to the atmosphere,

Table 5. Drag coefficients able to reproduce the secular semi-major axis decay of LARES from April 6, 2012 to December 25, 2015.

Atmospheric model	Drag coefficient C_D
JR-71	3.955
MSIS-86	3.713
MSISE-90	3.730
NRLMSISE-00	3.783
GOST2004	4.207
JB2008	3.051

Table 6. Drag coefficients able to reproduce the secular semi-major axis decay of Ajisai from April 6, 2012 to December 25, 2015.

Atmospheric model	Drag coefficient C_D
JR-71	3.420
MSIS-86	3.139
MSISE-90	3.131
NRLMSISE-00	3.194
GOST2004	3.340
JB2008	2.482

Table 7. Drag coefficients able to reproduce the secular semi-major axis decay of LARES from December 25, 2015 to October 26, 2018.

Atmospheric model	Drag coefficient C_D
JR-71	3.951
MSIS-86	4.003
MSISE-90	4.018
NRLMSISE-00	3.923
GOST2004	3.397
JB2008	2.635

Table 8. Drag coefficients able to reproduce the secular semi-major axis decay of Ajisai from December 25, 2015 to October 26, 2018.

Atmospheric model	Drag coefficient C_D
JR-71	3.846
MSIS-86	3.940
MSISE-90	3.928
NRLMSISE-00	3.820
GOST2004	3.086
JB2008	2.445

is the dissipation of orbital energy, leading to a gradual decrease in the satellite's semi-major axis. It is usual to express the drag force $\boldsymbol{F}_D$ in the form:

$$\vec{F}_D = -\frac{1}{2} C_D \frac{A}{M_S} \rho V^2 \frac{\vec{V}}{V}, \tag{1}$$

in which M_S is the mass of the satellite, ρ is the local atmospheric density, $\boldsymbol{V}$ is the velocity of the satellite relative to the atmosphere, A is the cross-sectional area of the satellite facing the airstream, and C_D is the drag coefficient (i.e., a dimensionless quantity that summarizes the interaction of the atmospheric molecules with the surface of the satellite exposed to the flow).[11,25,26)]

Having detected and measured the secular semi-major axis decay of LARES and Ajisai during the time spans of interest, and estimated the corresponding mean transverse accelerations T_D as described in Section 3, SATRAP was iteratively run – using the six thermospheric density models listed at the end of the introduction and taking into account the real evolution of the space weather conditions – until the "simulated" mean transverse accelerations reproduced the "measured" ones. This was obtained by iteratively changing the drag coefficients C_D for each density model, converging to the results shown in Tables 5, 6, 7 and 8. How the various C_D attained with the six density models compared among them, including their mean $\langle C_D \rangle$ and standard deviation σ, is detailed in the following.

For LARES, around the maximum of Solar Cycle 24, $\langle T_{exo} \rangle = 971\,\mathrm{K}$ and $\langle C_D \rangle = 3.740 \pm 0.385$ (1σ, $\approx 10\%$), while during the declining phase and the minimum of the cycle, $\langle T_{exo} \rangle = 796\,\mathrm{K}$ and $\langle C_D \rangle = 3.655 \pm 0.551$ (1σ, $\approx 15\%$). The highest average atmospheric density and therefore the lowest C_D (i.e., -18.4% with respect to $\langle C_D \rangle$ around the maximum and -27.9% during the declining phase and the minimum of the cycle) were predicted using JB2008. The lowest $\langle \rho \rangle$ and highest C_D were predicted using GOST2004 around the maximum (i.e., $+12.5\%$ with respect to $\langle C_D \rangle$) and using MSISE-90 during the declining phase and minimum of the cycle (i.e., $+10.0\%$ with respect to $\langle C_D \rangle$). Regarding the change of C_D resulting from the diminishing value of $\langle T_{exo} \rangle$, from 971 K to 796 K, it should be noted that, with JR-71, it basically displayed no variation (-0.1%) using GOST2004, and dropped about 19% and 14%, respectively, using JB2008. However, C_D increased nearly 4% using NRLMSISE-00 and almost 8% using MSIS-86 and MSISE-90.

Concerning Ajisai, around the maximum of Solar Cycle 24, $\langle T_{exo} \rangle = 960\,\mathrm{K}$ and $\langle C_D \rangle = 3.118 \pm 0.332$ (1σ, $\approx 11\%$), while during the declining phase and minimum of the cycle, $\langle T_{exo} \rangle = 784\,\mathrm{K}$ and $\langle C_D \rangle = 3.511 \pm 0.614$ (1σ, $\approx 17\%$). Again, the highest average atmospheric density and therefore the lowest C_D (i.e., -20.4% with respect to $\langle C_D \rangle$ around the maximum and -30.4% during the declining phase and minimum of the cycle) were predicted using JB2008, while the lowest $\langle \rho \rangle$ and highest C_D were predicted using JR-71 around the maximum (i.e., $+9.7\%$ with respect to $\langle C_D \rangle$) and using MSIS-86 during the declining phase and minimum of the cycle (i.e., $+12.2\%$ with respect to $\langle C_D \rangle$). Regarding the change in C_D resulting from the diminishing value of $\langle T_{exo} \rangle$, from 960 K to 784 K, it should be noted that it displayed a very small variation (-1.5%) using JB2008 and decreased less than 8% using GOST2004. However, C_D increased almost 12% using JR-71, nearly 20% using NRLMSISE-00, and more than 25% using MSIS-86 and MSISE-90.

Comparing the C_D estimates obtained for LARES and Ajisai, both passive spherical satellites at nearly the same altitude but with quite different orbital inclinations (i.e., about 70° and 50°, respectively) led to the following main conclusions:

1. All of the C_D found for Ajisai were systematically smaller than those of LARES using the same time intervals, space weather conditions and thermospheric density models.
2. Around the maximum of Solar Cycle 24, $\langle C_D \rangle$ for Ajisai

was 16.6% smaller compared to that of LARES.
3. During the decreasing phase and minimum of the cycle, $\langle C_D \rangle$ for Ajisai was 3.9% smaller compared to that of LARES.
4. When $\langle T_{exo} \rangle$ passed from ≈ 965 K to ≈ 790 K, LARES $\langle C_D \rangle$ decreased 2.3%, while Ajisai $\langle C_D \rangle$ increased 12.6%, leading to much better agreement between the mean drag coefficients of the two satellites.
5. The standard deviations of the C_D distributions were similar for the two satellites depending on the environmental conditions: 10–11% around the solar maximum, 15–17% during the declining phase and cycle minimum.
6. For LARES, when the solar activity diminished, the C_D of JR-71 basically remained the same, those of MSIS-86, MSISE-90 and NRLMSISE-00 increased, and those of GOST2004 and JB2008 decreased.
7. For Ajisai, when the solar activity diminished, the C_D of JB2008 remained substantially stable, those of JR-71, MSIS-86, MSISE-90 and NRLMSISE-00 increased, and that of GOST2004 decreased.
8. The JB2008 model predicted the highest atmospheric densities and lowest C_D for both satellites and space weather conditions.
9. In all of the cases, MSIS-86, MSISE-90 and NRLMSISE-00 produced very similar results, with maximum discrepancies of 3% or less; this was expected due to the common origin and heritage of the three models.

In any case, all of the changes and differences recorded in the models and among them are perfectly compatible with their known uncertainties and biases, even at the much lower altitudes (<1000 km) for which they were originally developed. Rather, their performances around 1500 km (i.e., at the altitudes of LARES and Ajisai) turned out to be surprisingly good and above expectations.

5. Neutral Drag Acceleration Components

The six thermospheric density models were used within SATRAP to compute the components of the neutral drag acceleration on both satellites in the reference system $R_D T_D W_D$.[29] The origin was in the center of mass of the satellites and the three orthogonal axes were aligned as follows: along the radial direction (R_D), from the center of the Earth to the satellite; normal to the orbit plane (W_D), in the direction of the osculating orbital angular momentum; and in the transverse direction (T_D), lying on the orbit plane 90° from the radial direction, nearly aligned with the satellite velocity vector. In each case, the drag coefficients were rescaled according to the results presented in Tables 5, 6, 7 and 8 in order to reproduce the observed secular semi-major axis decay and the corresponding drag-like perturbing acceleration with every atmospheric density model. The results of the simulations for each satellite and time interval are summarized in Figs. 9–20, where every neutral drag acceleration component is plotted for all six atmospheric density models.

Concerning R_D, the agreement among the models was quite good, both for LARES and Ajisai, and for "high" and "low" solar activity. $\langle R_D \rangle$ was very close to zero ($<2 \times 10^{-15}$ m/s^2) in any situation. For LARES, the greatest excursion of R_D was $\pm 8 \times 10^{-14}$ m/s^2 (Fig. 9) around the maximum of Solar Cycle 24, and $\pm 4 \times 10^{-14}$ m/s^2 (Fig. 10) during the declining phase and minimum of the same cycle. For Ajisai, the corresponding excursions of R_D were $\pm 1.5 \times 10^{-12}$ m/s^2 (Fig. 15) and $\pm 6 \times 10^{-13}$ m/s^2 (Fig. 16).

Regarding the widely prevalent acceleration component T_D, the agreement among the density models, apart from the same value of $\langle T_D \rangle$ needed for reproducing the secular

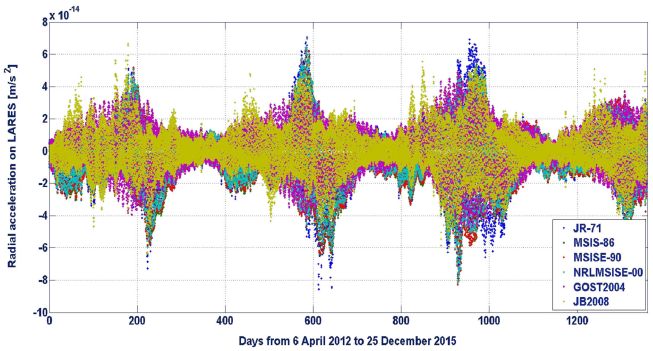

Fig. 9. Radial component (R_D) of the neutral drag acceleration on LARES from April 6, 2012 to December 25, 2015, computed using the six atmospheric density models.

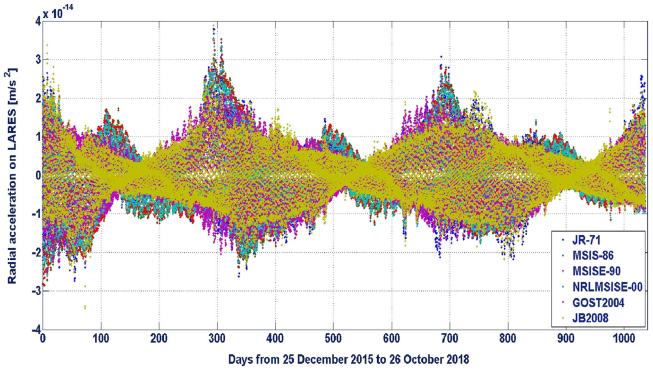

Fig. 10. Radial component (R_D) of the neutral drag acceleration on LARES from December 25, 2015 to October 26, 2018, computed using the six atmospheric density models.

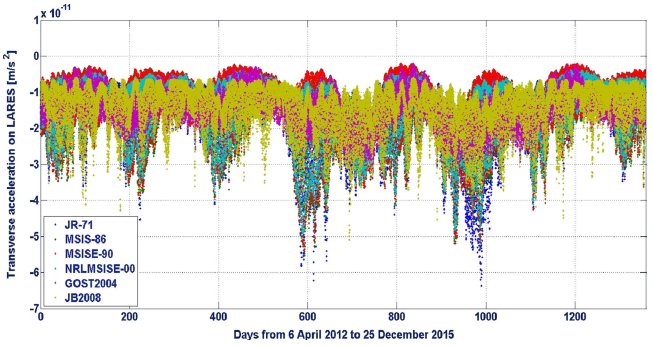

Fig. 11. Transverse component (T_D) of the neutral drag acceleration on LARES from April 6, 2012 to December 25, 2015, computed using the six atmospheric density models.

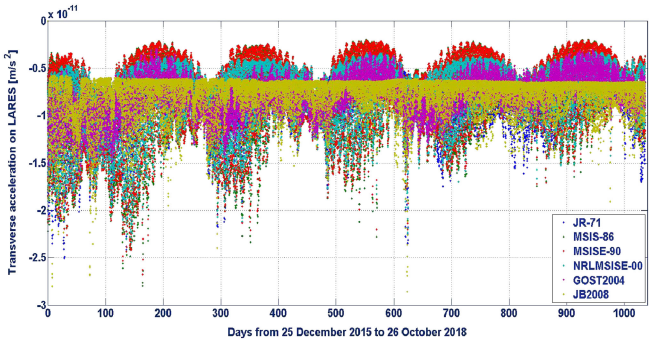

Fig. 12. Transverse component (T_D) of the neutral drag acceleration on LARES from December 25, 2015 to October 26, 2018, computed using the six atmospheric density models.

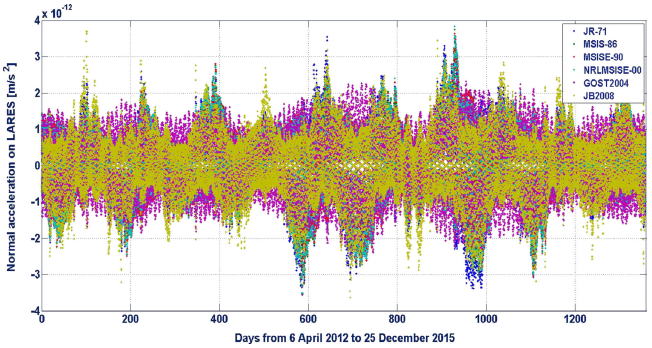

Fig. 13. Normal component (W_D) of the neutral drag acceleration on LARES from April 6, 2012 to December 25, 2015, computed using the six atmospheric density models.

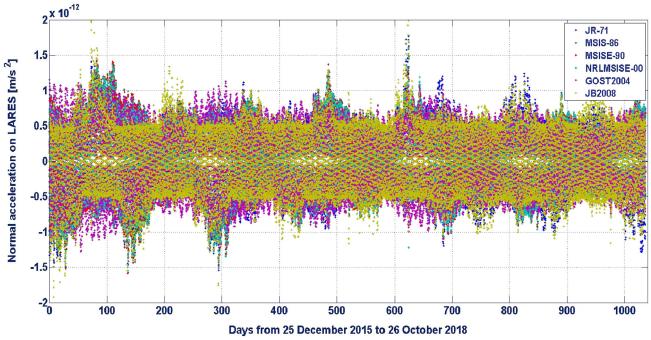

Fig. 14. Normal component (W_D) of the neutral drag acceleration on LARES from December 25, 2015 to October 26, 2018, computed using the six atmospheric density models.

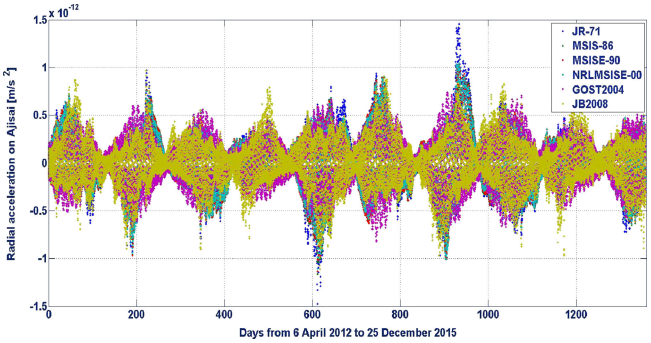

Fig. 15. Radial component (R_D) of the neutral drag acceleration on Ajisai from April 6, 2012 to December 25, 2015, computed using the six atmospheric density models.

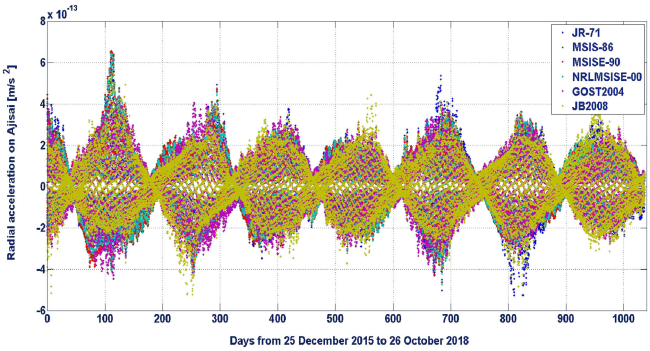

Fig. 16. Radial component (R_D) of the neutral drag acceleration on Ajisai from December 25, 2015 to October 26, 2018, computed using the six atmospheric density models.

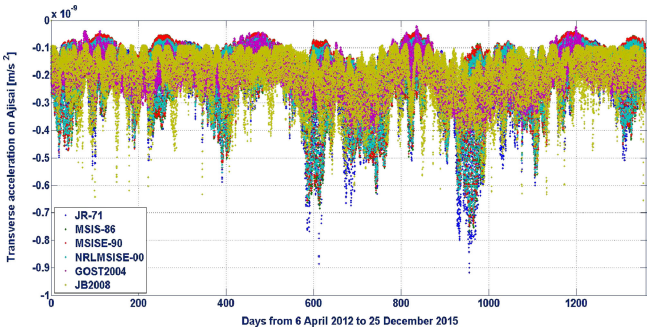

Fig. 17. Transverse component (T_D) of the neutral drag acceleration on Ajisai from April 6, 2012 to December 25, 2015, computed using the six atmospheric density models.

decay rate observed, was not nearly as good due to the presence of different periodic terms intrinsic to the definitions of the models themselves.[7,8] Due to their common heritage and development, MSIS-86, MSISE-90 and NRLMSISE-00 generally exhibited very good agreement, and in most cases JR-71 was not far from them. However, both GOST2004 and JB2008 displayed a quite distinctive behavior (see Figs. 11, 12, 17 and 18), further confirming the results already obtained around the maximum of Solar Cycle 24 and anticipated elsewhere.[7,8]

For LARES, the greatest excursion of T_D with respect to the average secular value $\langle T_D \rangle$ was $-5 \times 10^{-11}\,\mathrm{m/s^2}$ (Fig. 11) around the solar activity maximum and $-2 \times 10^{-11}\,\mathrm{m/s^2}$ (Fig. 12) during the declining phase and minimum of the same cycle. For Ajisai, the corresponding greatest excursions of T_D were $-7 \times 10^{-10}\,\mathrm{m/s^2}$ (Fig. 17) and $-3 \times 10^{-10}\,\mathrm{m/s^2}$ (Fig. 18). However, GOST2004 always exhibited much smaller fluctuations (i.e., by a factor of 3–7) and relatively symmetrical long-period oscillations; a pattern not shared by any of the other models.

Concerning W_D, the agreement among the models was much better, both for LARES and Ajisai, and for "high" and "low" solar activity. However, JB2008 and, in particular, GOST2004, again exhibited rather distinct features. $\langle W_D \rangle$

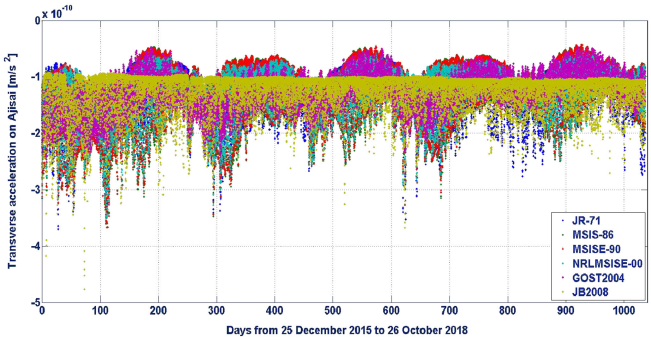

Fig. 18. Transverse component (T_D) of the neutral drag acceleration on Ajisai from December 25, 2015 to October 26, 2018, computed using the six atmospheric density models.

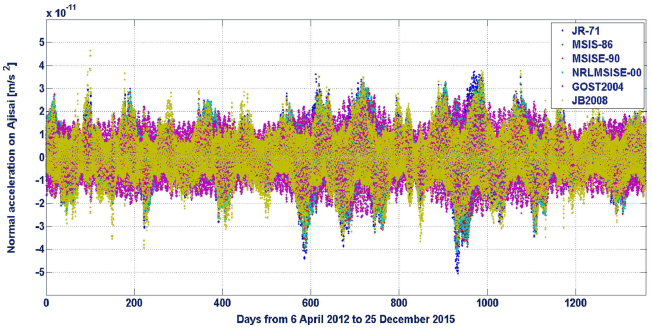

Fig. 19. Normal component (W_D) of the neutral drag acceleration on Ajisai from April 6, 2012 to December 25, 2015, computed using the six atmospheric density models.

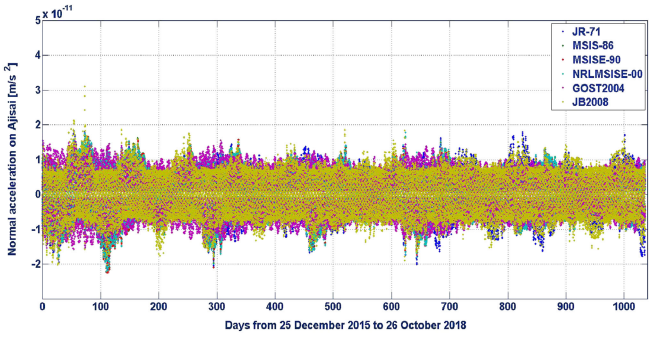

Fig. 20. Normal component (W_D) of the neutral drag acceleration on Ajisai from December 25, 2015 to October 26, 2018, computed using the six atmospheric density models.

was very close to zero (i.e., $<8 \times 10^{-14}$ m/s^2 for Ajisai and $<8 \times 10^{-15}$ m/s^2 for LARES) under all space environment conditions. For LARES, the greatest excursion of W_D was $\pm 4 \times 10^{-12}$ m/s^2 (Fig. 13) around the maximum of Solar Cycle 24 and $\pm 2 \times 10^{-12}$ m/s^2 (Fig. 14) during the declining phase and minimum of the same cycle. For Ajisai, the equivalent excursions of W_D were $\pm 5 \times 10^{-11}$ m/s^2 (Fig. 19) and $\pm 2 \times 10^{-11}$ m/s^2 (Fig. 20).

6. Biases of the Density Models

In order to further investigate the neutral atmosphere at the altitude of LARES and Ajisai and evaluate the performances of the six atmospheric models used in the present analysis, an attempt was made to estimate the "physical" drag coefficient C_{DF} of the two satellites. When $V > V_m$, as in the cases considered here,[‡] C_{DF} can be computed as follows[30–32]:

$$C_{DF} = \delta \left[2 + \frac{4}{3}\left(\frac{V_m}{V}\right)^2 - \frac{2}{15}\left(\frac{V_m}{V}\right)^4 \right], \tag{2}$$

where

$$V_m = \sqrt{\frac{2RT}{10^3 M}}, \tag{3}$$

$$\delta = 1 + \frac{4}{9}\sqrt{1-\alpha}, \tag{4}$$

and

$$\alpha = \frac{3.8\mu}{(1+\mu)^2}. \tag{5}$$

The computation was independently carried out using an ad hoc software routine for each of the relevant atomic species (i.e., H, He and O) of the atmosphere at the altitude of interest. The satellite velocity V with respect to the atmosphere was computed using the orbit parameters, while the atmospheric temperature T and composition were estimated using the NRLMSISE-00 model. All of the other parameters were derived from these basic inputs according to their definitions or Eqs. (3)–(5). For the numerical constant appearing in the numerator of Eq. (5), the value proposed by Jacchia (i.e., 3.8) was adopted.[32] Moreover, the chemical composition of the surface of LARES was supposed to be 26% silicon dioxide (SiO_2) and 74% tungsten (W). Finally, for each satellite and time interval considered, the comprehensive physical drag coefficient applicable to the neutral atmosphere as a whole was obtained as follows:

$$C_{DF} = \frac{C_{D\mathrm{H}} n_{\mathrm{H}} + C_{D\mathrm{He}} n_{\mathrm{He}} + C_{D\mathrm{O}} n_{\mathrm{O}}}{n_{\mathrm{H}} + n_{\mathrm{He}} + n_{\mathrm{O}}}. \tag{6}$$

Table 9. Mean physical drag coefficients estimated for LARES ($\langle h \rangle = 1454$ km, $i = 69.5°$) and Ajisai ($\langle h \rangle = 1494$ km, $i = 50.0°$) as a function of the mean exospheric temperature.

Satellite	$\langle T_{exo} \rangle$	$\langle C_{DF} \rangle$
LARES	971 K	3.181
Ajisai	960 K	3.164
LARES	796 K	3.276
Ajisai	784 K	3.277

Table 9 shows the mean physical drag coefficients obtained. Under the same space weather conditions, they turned out to be very similar. The difference between LARES and Ajisai was about 0.5% around the maximum of Solar Cycle 24 and just 0.05% during the declining phase and low minimum of the same cycle. The $\langle C_{DF} \rangle$ of both satellites increased more or less 3% in response to the atmospheric

[‡]Even for atomic hydrogen, the faster species, $V > V_m$ by a factor ~50 or more.

Table 10. Estimated mean density $\langle\rho\rangle$ biases of the atmospheric models for $\langle h\rangle = 1454$ km, $i = 69.5^\circ$ and $\langle T_{exo}\rangle = 971$ K (LARES, from April 6, 2012 to December 25, 2015).

Atmospheric model	Mean density $\langle\rho\rangle$ bias (%)
JR-71	−24.3
MSIS-86	−16.7
MSISE-90	−17.3
NRLMSISE-00	−18.9
GOST2004	−32.2
JB2008	+4.09

Table 11. Estimated mean density $\langle\rho\rangle$ biases of the atmospheric models for $\langle h\rangle = 1494$ km, $i = 50.0^\circ$ and $\langle T_{exo}\rangle = 960$ K (Ajisai, from April 6, 2012 to December 25, 2015).

Atmospheric model	Mean density $\langle\rho\rangle$ bias (%)
JR-71	−8.08
MSIS-86	+0.80
MSISE-90	+1.05
NRLMSISE-00	−0.94
GOST2004	−5.55
JB2008	+21.6

Table 12. Estimated mean density $\langle\rho\rangle$ biases of the atmospheric models for $\langle h\rangle = 1454$ km, $i = 69.5^\circ$ and $\langle T_{exo}\rangle = 796$ K (LARES, from December 25, 2015 to October 26, 2018).

Atmospheric model	Mean density $\langle\rho\rangle$ bias (%)
JR-71	−20.6
MSIS-86	−22.2
MSISE-90	−22.7
NRLMSISE-00	−19.8
GOST2004	−3.71
JB2008	+19.6

Table 13. Estimated mean density $\langle\rho\rangle$ biases of the atmospheric models for $\langle h\rangle = 1494$ km, $i = 50.0^\circ$ and $\langle T_{exo}\rangle = 784$ K (Ajisai, from December 25, 2015 to October 26, 2018).

Atmospheric model	Mean density $\langle\rho\rangle$ bias (%)
JR-71	−17.4
MSIS-86	−20.2
MSISE-90	−19.9
NRLMSISE-00	−16.6
GOST2004	+5.83
JB2008	+25.4

changes, from a He-dominated to a H-dominated composition when $\langle T_{exo}\rangle$ diminished from ≈ 965 K to ≈ 790 K.

It was assumed that the theoretical values of $\langle C_{DF}\rangle$ obtained correctly represent the real mean drag coefficients of the two satellites. Comparing them with the "observed" values listed in Tables 5, 6, 7 and 8 allowed a detailed evaluation of the overall performances of the atmospheric density models at altitudes of 1450–1500 km as a function of solar activity and satellite orbit inclination. The further relevance of the latter parameter is derived from the fact that LARES, with its greater inclination, probes medium- to high-latitude atmospheric regions (i.e., $50^\circ < |\varphi| < 70^\circ$), which are inaccessible to Ajisai and can respond differently to space weather and solar activity disturbances. The comparison between "observed" and "theoretical" mean drag coefficients led to estimation of the average density biases displayed in Tables 10, 11, 12 and 13. A positive value implies that the model overestimates the actual average density, while a negative value means that the model underestimates it.

Around the maximum of Solar Cycle 24, along the orbits of LARES (see Table 10), characterized by $0^\circ \leq |\varphi| < 70^\circ$, five out of six atmospheric models significantly underestimated the average atmospheric density. MSIS-86, MSISE-90 and NRLMSISE-00, as expected, provided very similar results, with a density underestimation of 17–19%. For JR-71, it neared 25%, while it exceeded 30% for GOST2004. The best model as far as the average atmospheric density was concerned was JB2008, which overestimated the density by only 4%. Always around the maximum of Solar Cycle 24, but along the orbits of Ajisai (see Table 11), characterized by $0^\circ \leq |\varphi| \leq 50^\circ$, the situation was completely different. In fact, JB2008 was the worst model, overestimating the mean density by nearly 22%. GOST2004 and JR-71 underestimated the actual atmospheric density by a relatively small amount, around 6% and 8%, respectively. The three models sharing a common origin and development (i.e., MSIS-86, MSISE-90 and NRLMSISE-00), gave results that were quite accurate, with biases of more or less 1%. The significant differences between the results obtained for LARES and Ajisai around the solar maximum might suggest that all of the density models considered in the present analysis are not able to accurately describe latitude dependent effects, probably more pronounced at high φ values during periods of high solar activity.[8)]

During the declining phase and minimum of Solar Cycle 24, these latitude-dependent density biases mostly disappeared and all of the models provided rather similar estimates, with the possible exception of GOST2004, for both LARES and Ajisai (see Tables 12 and 13). In both cases, GOST2004 was by far the best model as far as the average atmospheric density was concerned. It underestimated the density by less than 4% along the trajectory of LARES and overestimated it by less than 6% along the trajectory of Ajisai. On the other hand, JR-71, MSIS-86, MSISE-90 and NRLMSISE-00 underestimated the mean density by amounts between more than 16% and less than 23% for both satellites. Lastly, JB2008 overestimated the average density by about 20–25%.

7. Conclusions and Future Work

The extensive set of analyses carried out allowed use of the passive spherical satellites LARES and Ajisai as powerful tools to probe the neutral atmosphere properties at altitudes of 1450–1500 km during Solar Cycle 24, both around the maximum and during the declining phase and deep minimum. The six thermospheric models used in this study (i.e., JR-71, MSIS-86, MSISE-90, NRLMSISE-00, GOST2004 and JB2008) were developed for $h < 1000$ km. Even so, they exhibited quite satisfactory levels of performance and varia-

bility as functions of the varying space weather conditions and orbit geometry with respect to the atmosphere. In other words, the comparative analyses and average density biases estimated were fully compatible with the known uncertainties and discrepancies of the models. Furthermore, the overall picture was not significantly worse than that observed at the lower altitudes for which those same models were developed, and mostly tested, so far.[33–36] At the altitudes of LARES and Ajisai, these results alone are not enough to suggest the action of other dissipative non-gravitational perturbations capable of producing a significant fraction of the secular decay in the semi-major axis observed for the two satellites.[7,8]

It should be also pointed out that the results obtained for Ajisai using the three oldest models (i.e., JR-71, MSIS-86 and MSISE-90) were in qualitative agreement with those obtained during Solar Cycle 22 from April 24, 1988 to June 30, 1997,[24,25] even if that cycle was much more intense than the current one and the periods considered are then not directly comparable.

Among the six thermospheric models used, none could be considered unconditionally the best, confirming a situation already familiar at lower altitudes. The outcome, in fact, depended on the specifics of the circumterrestrial environment determined by solar activity and space weather, as well as by the regions of the atmosphere crossed by the satellites. Looking at the mean density biases estimated in this study, JB2008 seemed the most accurate around the solar maximum for orbits reaching a geocentric latitude close to 70°, while MSIS-86, MSISE-90 and NRLMSISE-00 provided the best results when the ceiling latitude was 50°. During the diminishing phase and minimum of the solar cycle, on the other hand, the most accurate model was GOST2004 irrespective of the latitudes crossed by the satellites.

A further result of the analysis was that all of the models displayed a significant and roughly comparable latitude dependent bias around the solar maximum.[8] In other words, maintaining the same nearly circular orbit at the same altitude, but passing from $i \approx 50^\circ$ to $i \approx 70^\circ$, would have led to an average deficit in the computed mean atmospheric density of about 19% compared to the real value.

According to the predictions issued in April 2019 by an international panel of experts gathered by the National Oceanic and Atmospheric Administration (NOAA), Solar Cycle 24, already one of the feeblest on record, will reach its lowest point sometime between July 2019 and September 2020, followed by a slow recovery toward solar maximum in 2023–2026.[37] Solar Cycle 25 is expected to be very similar to Cycle 24, with a further really weak maximum, preceded by a long and very deep minimum.[37]

Therefore, in the coming decade there will be the possibility to additionally extend and possibly confirm the analysis outlined in this study, again using LARES and Ajisai as atmospheric density probes. Of particular scientific relevance will be investigating the environmental conditions during the long and deep minimum between Cycles 24 and 25. Additionally, repetition of the analysis during the maximum of Cycle 25 will be important in order to confirm the latitude-dependent density bias of the models. A supplementary improvement could be represented by including the study of additional state-of-the-art thermospheric density models.

Acknowledgments

This work was carried out in the framework of the Laser Ranged Satellites Experiment (LARASE) and was supported in part by the National Scientific Commission II (CSNII) on Astroparticle Physics Experiments of the National Institute of Nuclear Physics (INFN), in Italy. The authors are also indebted to the International Laser Ranging Service (ILRS) for providing high-quality laser ranging data of the LARES satellite, to the US Space Track Organization for making available the Two-Line Elements of LARES and Ajisai used in this study, and to NASA/GSFC for the software package GEODYN II.

Concerning the thermospheric density models implemented in the ISTI/CNR software tool SATRAP, the authors are indebted to Prof. Andrey Nazarenko, who provided the documentation and useful support during implementation of the Russian model GOST2004; to the Naval Research Laboratory for the Fortran source of the MSIS-86, MSISE-90 and NRLMSISE-00 models; to Space Environment Technologies for the Fortran source and the solar and geomagnetic activity indices of the JB2008 model; and to NOAA and The Solar Terrestrial Activity Report by Jan Alvestad for the observed solar and geomagnetic indices.

References

1) Lucchesi, D., Anselmo, L., Bassan, M., Pardini, C., Peron, R., Pucacco, G., and Visco, M.: Testing the Gravitational Interaction in the Field of the Earth via Satellite Laser Ranging and the Laser Ranged Satellites Experiment (LARASE), *Class. Quantum Grav.*, **32** (2015), 155012, 50 pp.
2) Ciufolini, I., Paolozzi, A., Pavlis, E. C., Koenig, R., Ries, J., Gurzadyan, V., Matzner, R., Penrose, R., Sindoni, G., Paris, C., Khachatryan, H., and Mirzoyan, S.: A Test of General Relativity Using the LARES and LAGEOS Satellites and a GRACE Earth Gravity Model. Measurement of Earth's Dragging of Inertial Frames, *Eur. Phys. J. C*, **76** (2016), 120, 7 pp.
3) Lucchesi, D. M., Magnafico, C., Peron, R., Visco, M., Anselmo, L., Pardini, C., Bassan, M., Pucacco, G., and Stanga, R.: The LARASE Research Program. State of the Art on Modelling and Measurements of General Relativity Effects in the Field of the Earth: A Preliminary Measurement of the Lense-Thirring Effect, Proceedings of 4th IEEE International Workshop on Metrology for Aerospace, Padua, Italy, 2017, pp. 131–145.
4) Lucchesi, D. M., Magnafico, C., Peron, R., Visco, M., Anselmo, L., Pardini, C., Bassan, M., Pucacco, G., and Stanga, R.: New Measurements of Gravitation in the Field of the Earth and the LARASE Experiment, Proceedings of 5th IEEE International Workshop on Metrology for Aerospace, Rome, Italy, 2018, pp. 209–215.
5) Paolozzi, A. and Ciufolini, I.: LARES Successfully Launched in Orbit: Satellite and Mission Description, *Acta Astronaut.*, **91** (2013), pp. 313–321.
6) Pearlman, M. R., Degnan, J. J., and Bosworth, J. M.: The International Laser Ranging Service, *Adv. Space Res.*, **30** (2002), pp. 135–143.
7) Pardini, C., Anselmo, L., Lucchesi, D. M., and Peron, R.: On the Secular Decay of the LARES Semi-Major Axis, *Acta Astronaut.*, **140** (2017), pp. 469–477.
8) Pardini, C., Anselmo, L., Lucchesi, D. M., and Peron, R.: Neutral Atmosphere Drag at the Altitude of LARES and Ajisai, 69th International Astronautical Congress, Bremen, Germany, IAC-18, C1,1,12x45729, 2018.
9) Sengoku, A., Cheng, M. K., and Schutz, B. E.: Anisotropic Reflection Effect on Satellite Ajisai, *J. Geod.*, **70** (1995), pp. 140–145.

10) Pardini, C. and Anselmo, L.: SATRAP: Satellite Reentry Analysis Program, CNUCE/CNR Internal Report C94-17, 1994.
11) Pardini, C., Moe, K., and Anselmo, L.: Thermospheric Density Model Biases at the 23rd Sunspot Maximum, *Planet. Space Sci.*, **67** (2012), pp. 130–146.
12) Cappellari, J. O., Velez, C. E., and Fuchs, A. J. (Eds.): Mathematical Theory of the Goddard Trajectory Determination System, NASA/GSFC Report X-582-76-77, 1976, pp. 4.33–4.53.
13) Hedin, A. E.: MSIS-86 Thermospheric Model, *J. Geophys. Res.*, **92** (1987), pp. 4649–4662.
14) Hedin, A. E.: Extension of the MSIS Thermosphere Model into the Middle and Lower Atmosphere, *J. Geophys. Res.*, **96** (1991), pp. 1159–1172.
15) Picone, J. M., Hedin, A. E., Drob, D. P., and Lean, J.: NRLMSISE-00 Empirical Model: Comparisons to Data and Standard Models, AAS Paper 01-394, 2001.
16) Picone, J. M., Hedin, A. E., Drob, D. P., and Aikan, A. C.: NRLMSISE-00 Empirical Model of the Atmosphere: Statistical Comparisons and Scientific Issues, *J. Geophys. Res.*, **107** (2002), A12: 1468, 16 pp.
17) Volkov, I. I.: Earth's Upper Atmosphere Density Model for Ballistic Support of the Flight of Artificial Earth Satellites, GOST R 25645.166-2004, 2004.
18) Bowman, B. R., Tobiska, W. K., Marcos, F. A., Huang, C. Y., Lin, C. S., and Burke, W. J.: A New Empirical Thermospheric Density Model JB2008 Using New Solar and Geomagnetic Indices, AIAA Paper 2008-6438, 2008.
19) Tobiska, W. K., Bouwer, S. D., and Bowman, B. R.: The Development of New Solar Indices for Use in Thermospheric Density Modeling, *J. Atmos. Sol.-Terr. Phy.*, **70** (2008), pp. 803–819.
20) Space Environment Technologies: The Jacchia-Bowman 2008 Empirical Thermospheric Density Model, http://sol.spacenvironment.net/jb2008/ (accessed April 1, 2019).
21) Putney, B., Kolenkiewicz, R., Smith, D., Dunn, P., and Torrence, M. H.: Precision Orbit Determination at the NASA Goddard Space Flight Center, *Adv. Space Res.*, **10** (1990), pp. 197–203.
22) Pavlis, D. E., Luo, S., Dahiroc, P., McCarthy, J. J., and Luthcke, S. B.: GEODYN II Operations Manual, NASA/GSFC and STX Systems Corporation, 1998.
23) Beutler, G.: *Methods of Celestial Mechanics, Vol. I: Physical, Mathematical, and Numerical Principles*, Springer-Verlag, Berlin & Heidelberg, 2005, pp. 230–231.
24) Pardini, C. and Anselmo, L.: Calibration of Semi-Empirical Atmosphere Models through the Orbital Decay of Spherical Satellites, AAS Paper 99-384, 1999.
25) Pardini, C. and Anselmo, L.: Comparison and Accuracy Assessment of Semi-Empirical Atmosphere Models through the Orbital Decay of Spherical Satellites, *J. Astronaut. Sci.*, **49** (2001), pp. 255–268.
26) Pardini, C., Tobiska, W. K., and Anselmo, L.: Analysis of the Orbital Decay of Spherical Satellites Using Different Solar Flux Proxies and Atmospheric Density Models, *Adv. Space Res.*, **37** (2006), pp. 392–400.
27) Hoots, F. R. and Roehrich, R. L.: Models for Propagation of NORAD Elements Sets, Spacetrack Report No. 3, 1980.
28) Vallado, D. A. and Crawford, P.: SGP4 Orbit Determination, AIAA Paper 2008-6770, 2008.
29) Roy, A. E.: *Orbital Motion*, Third Edition, Adam Hilger, Bristol, 1988, pp. 191–192.
30) Afonso, G., Barlier, F., Berger, C., Mignard, F., and Walch, J. J.: Reassessment of the Charge and Neutral Drag of LAGEOS and Its Geophysical Implications, *J. Geophys. Res.*, **90B** (1985), pp. 9381–9398.
31) Bowman, B. R.: Atmospheric Density Variations at 1500–4000 km Height Determined from Long Term Orbit Perturbation Analysis, AAS Paper 01-132, 2001.
32) Zarrouati, O.: *Trajectoires Spatiales*, Cepadues Editions, Toulouse, 1987, p. 118 (in French).
33) Montenbruck, O. and Gill, E.: *Satellites Orbits—Models, Methods, and Applications*, Corrected Second Printing, Springer, Berlin, 2001, pp. 98–102.
34) Yurasov, V. S., Nazarenko, A. I., Cefola, P. J., and Alfriend, K. T.: Results and Issues of Atmospheric Density Corrections, AAS Paper 04-305, 2004.
35) Volkov, I. I., Semenov, A. I., and Suevalov, V. V.: Analysis of Thermospheric Density Variations Neglected in Modern Atmospheric Models Using Accelerometer Data, *Sol. Syst. Res.*, **42** (2008), pp. 51–62.
36) CIRA-2012 International Working Group: COSPAR International Reference Atmosphere 2012 (CIRA-2012)—Models of the Earth's Upper Atmosphere, Version 1.0, 2012.
37) Phillips, T.: Experts Predict a Long, Deep Solar Minimum, http://spaceweather.com/ (accessed April 12, 2019).

Kiyokazu Koga
Associate Editor